Journal of Structural Geology 54 (2013) 174–179

Contents lists available at SciVerse ScienceDirect

Journal of Structural Geology

journal homepage: www.elsevier.com/locate/jsg

Fold dating: A new Ar/Ar illite dating application to constrain the age of deformation in shallow crustal rocks

Elisa Fitz-Diaz*, Ben van der Pluijm

Department of Earth & Environmental Sciences, University of Michigan, 1100 North University Ave., Ann Arbor, MI 48109-1005, USA

ARTICLE INFO

Article history:
Received 13 March 2013
Received in revised form
28 May 2013
Accepted 30 May 2013
Available online 15 June 2013

Keywords:
Fold dating
Illite
Ar–Ar dating
Basin inversion

ABSTRACT

We propose a deformation dating method that combines XRD quantification and Ar chronology of submicroscopic illite to determine the absolute ages of folds that contain clay-bearing layers. Two folds in the frontal segment of the Mexican Fold-Thrust Belt (MFTB), which was deformed from Late Cretaceous to Eocene, are used to illustrate the method and its future potential.

Variations in mineral composition, illite-polytype, crystallite-size (CS) and Ar total gas ages were analyzed in the limbs and hinge of two mesoscopic folds. This analysis examines potential effects of strain variation on illitization and the Ar isotopic system along folded layers, versus possible regional thermal overprints. The Ar total-gas ages for 9 samples in Fold 1 vary between 48.4 and 43.9 Ma. The % of $2M_1$ (detrital) illite vs. Ar total-gas ages tightly constrains the age of folding at 43.5 ± 0.3 Ma. Nine ages from three samples in Fold 2 range from 76.2 to 62.7 Ma, which results in a folding age of 63.9 ± 2.2 Ma. Both ages are in excellent agreement with more broadly constrained stratigraphic timing. The method offers a novel approach to radiometric dating of clay-bearing folds formed at very low-grade metamorphic conditions, and has the potential to constrain dates and rates of regional and local deformation along and across foreland orogenic belts.

1. Introduction

Despite the fact that folds are among the most common deformation features in the upper crust, and that many aspects of their kinematic and thermodynamic evolution have been thoroughly addressed over the past decades (see Hudleston and Treagus, 2010; Hobbs et al., 2011 for recent summaries), direct dating of folding at low-grade metamorphic conditions has remained a challenge. The method described in this paper attempts to address this critical gap in structural geology and regional tectonic analysis by applying a method that is similar to Ar illite dating in fault gouge (Haines and van der Pluijm, 2008). Whereas fault-gouge analysis capitalizes on slip and chemical processes along major faults that may be regional conduits and foci of deformation (e.g., Vrolijk and van der Pluijm, 1999), fold analysis typically reflects local conditions in the host rock, such as within thrust sheets (e. g. Fitz-Diaz et al., 2011a, 2012). The reasons why illite is targeted to obtain ages of deformation in shallow crustal rocks are: (1) illite precipitates from fluids interacting with host rock during burial and/or deformation at low temperatures (Dong et al., 1997; Pevear, 1999; van der Pluijm et al., 2001; Rousset and Clauer, 2003; Clauer et al., 2008; Surace et al., 2011; Verdel et al., 2011); (2) Illite contains potassium, which is radiogenic; and (3) the diffusion of radiogenic argon (Ar) in the illite crystal structure is very slow at low temperatures (Dong et al., 1995; Clauer et al., 1997). In this study, we targeted mesoscopic folds of the same clay-rich unit in a single depositional environment, and followed three steps in our analysis: (1) establishing the tectonic/structural setting of folding; (2) extracting and characterizing different illite size fractions from samples collected along a fold; and, (3) obtaining Ar ages from several illite size fractions of each fold.

The aim of this short paper is to offer a first report on our progress with fold dating using Ar-encapsulation dating and polytype quantification of illite. The regional implications of these ages for the evolution of the MFTB are outside the scope of this report, and will be discussed in a future contribution.

2. Geological setting

The Mexican Fold-Thrust Belt (MFTB) is a southern portion of the Rocky Mountains Fold-Thrust Belt and mostly deforms cretaceous carbonate sequences (Fig. 1, Fitz-Diaz et al., 2011a). Folded

* Corresponding author.
E-mail addresses: fitzdiaz@umich.edu, fitzde@gmail.com (E. Fitz-Diaz), vdpluijm@umich.edu (B. van der Pluijm).

0191-8141/$ – see front matter © 2013 Elsevier Ltd. All rights reserved.
http://dx.doi.org/10.1016/j.jsg.2013.05.011

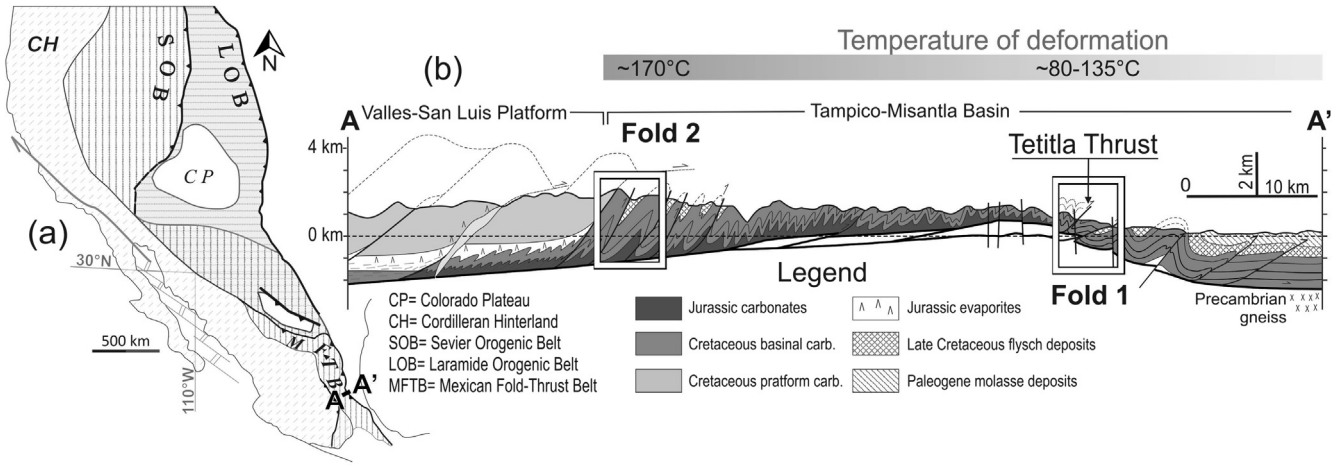

Fig. 1. (a) Tectonic map of southwestern North America, showing the location of the section where the Tampico-Misantla Basin is deformed by the Mexican Fold-Thrust Belt (MFTB). (b) Regional cross-section of the MFTB in central México, showing the location of the studied folds in the Tampico-Misantla Basin (modified from Fitz-Díaz et al., 2011a).

shale layers in the frontal MFTB are interbedded with limestone layers containing planktonic foraminifera and chert bands. This sequence, the Ahuacatlan-Chapulhuacan Fm., is the characteristic unit of the Albian-Cenomanian Tampico-Misantla Basin (TMB) in eastern Mexico (Suter, 1987). Folds 1 and 2 are found in the easternmost edge of the MFTB, in the footwall of the Tetitla Thrust (Fig. 1). Unlike platformal carbonates in the adjacent Valles-San Luis Potosí, which accommodated shortening primarily by thrust imbrication, thrust sheets with the basinal carbonate sequences experienced internal deformation by folding during a main local deformation phase (D1), with a direction of transport toward the ENE during the Late Cretaceous-Paleocene (Fitz-Diaz et al., 2012). These folds involve Campaninan-Maastrichtian turbidites (Pessagno, 1969; López-Oliva et al., 1999). A less intense and also east-verging shortening phase (D2) deformed these rocks in the Late Eocene (Alzaga-Ruiz et al., 2009), to the east of the Tetitla Thrust. Besides Cretaceous carbonates, D2 folds also deform Paleocene-Early Eocene units and the K-T angular unconformity (López-Oliva et al., 1999) in the front of the MFTB, constraining the age of deformation.

Within a shallow fold-thrust belt, such as the MFTB, the temperature of deformation is mostly related to the geothermal gradient, (Dahlen and Barr, 1989) and can therefore be considered constant within a slowly deforming mesoscopic rock-volume, as any contribution by frictional heating is negligible (Cardwell et al., 1978). Based on fluid-inclusion analysis and vitrinite reflectance, estimates for the temperature conditions of deformation range between ~80 and 170 °C in the exposed rocks of the TMB (Gray et al., 2001; Fitz-Díaz et al., 2011b; Ortega-Flores, 2011). This temperature window is optimal for illite precipitation (e.g., Merriman and Peacor, 1999).

Fold 1 is an inclined, open, quasi-symmetrical chevron fold, with an axial plane dipping 60° toward 245°, and with an axis plunging 6° to the NW (Fig. 2a). It has an interlimb angle of approximately 80°, which implies a limb rotation of 50°, assuming that the layers were horizontal prior to folding. Ramsay's (1974) theory suggests that is enough amount to induce significant amounts of shear parallel to the bedding in the thinner, incompetent layers. The thickness of the competent layers range from 20 to 50 cm but each layer has constant thickness around the fold. The thickness of incompetent layers range from 2 to 40 cm, and individual layers thicken in the in the hinge zone and thin in the limbs. Besides extensional veins in the hinge zone, the competent layers show no evidence of internal deformation, whereas the incompetent layers show a strong continuous cleavage in the limbs and spaced cleavage associated with micro-folds in the hinge.

Fold 2 is an inclined, tight, asymmetrical chevron fold with an axial plane dipping 45°–220°, an axis plunging 9° to the NW, and an interlimb angle of 40° (Fig. 2b). Competent layers are slightly thicker in the hinge zone compared to the limbs. Analogous to Fold 1, shale layers are thinner in limbs showing a continuous cleavage, and are thicker in the hinge zone with a spaced crenulation cleavage. This field-based distinction between layer thickness and rock fabric (e. g. crenulation vs. continuous cleavage) in the hinge and limbs was the motivation for a detailed analysis of shale layers because it was hoped that neo-formation of illite during folding was structurally dependent on thickness/deformation history differences around the folded layers.

3. Method

Our method involves several steps, as shown in Fig. 3: I) selection of fold in the TMB at a structurally shallow and less deformed part of the MFTB on its eastern edge; II) kinematic analysis of the folds; III) testing for variable illitization in the limbs and hinge; IV) collection of three, 300 g samples from clay-rich layers in the limbs and hinge of each fold (Fig. 2); V) XRD analyses and illite quantification of whole-rock and clay size-fractions (<2 μm/bulk, and <0.05 μm/fine, 0.05–0.2 μm/fine-medium, 0.2–1 μm/medium-coarse, 1–2 μm/coarse) to characterize illite and to examine for other potassium-bearing phases that could be present; and VI) radiometric ages determined using the vacuum-encapsulated, Ar-illite dating method (Dong et al., 1995; van der Pluijm et al., 2001).

Step V includes high-resolution XRD-analyses in air-dried and glycolated oriented samples that permit the determination of the illite-crystallinity index (IC; Kübler, 1968) and % smectite in the illite/smectite ratio (Moore and Reynolds, 1997). Clay separation involved rock crushing, dispersion of powder in de-ionized water in an ultrasonic bath, separation of different clay size-fractions (<0.05 μm, fine; 0.05–0.2 μm, medium-fine; 0.2–1 μm –medium-coarse; 1–2 μm, coarse and <2 μm, bulk clay size-fraction) by centrifuge, and sample drying. No chemical treatment that could affect the chemistry of the clay was applied to the samples. The IC was calibrated following Warr and Rice's (1994) method and standards. The average crystallite-size (CS), i.e., crystallite thickness, from each size fraction is determined from the IC by the Scherrer equation (Moore and Reynolds, 1997). The proportions of

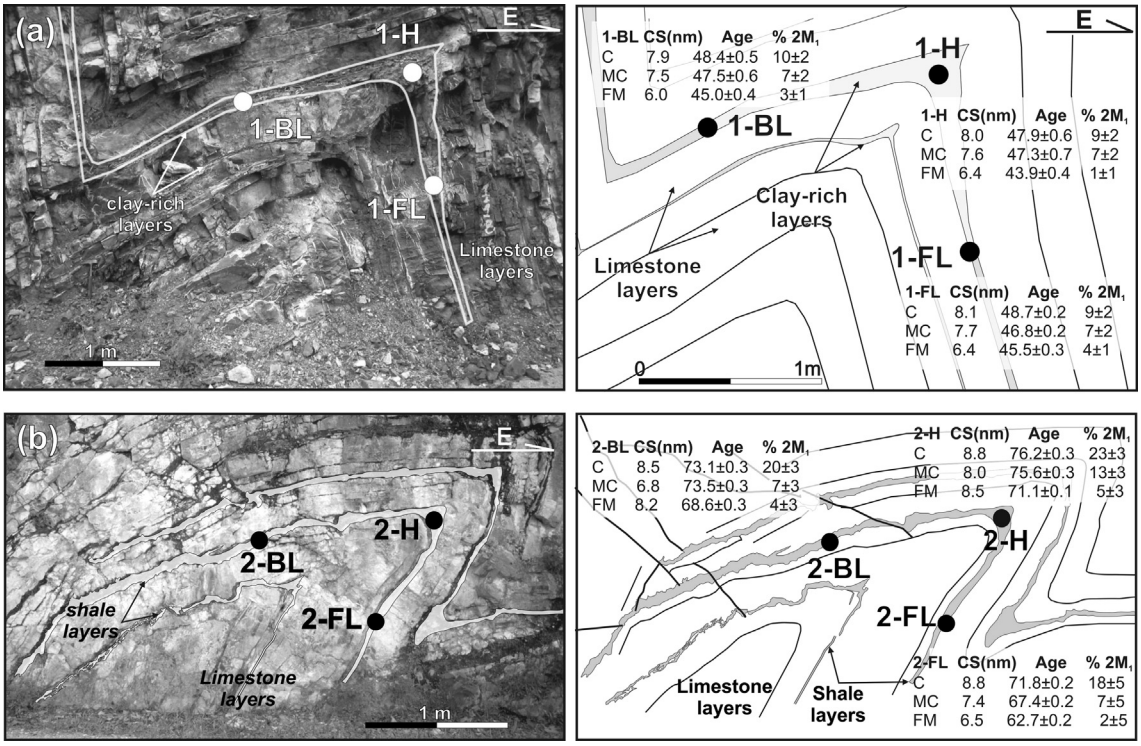

Fig. 2. (a) Photograph of Fold 1, showing its geometry elements and the sample location for the clay-rich layers, and sketch of the fold showing distribution of crystallite-size (CS), ages and % $2M_1$ estimates within the structure. (b) Photograph of Fold 2 and sketch with results, as above.

$2M_1$ (detrital) and $1M_d$ (authigenic) illite in the samples are determined by comparing high-resolution XRD patterns measured in randomly-oriented powder samples with model patterns in WILDFIRE (Reynolds, 1992; Haines and van der Pluijm, 2008).

An accurate interpretation of the age of deformation, Step V, requires Ar ages to be determined in different clay size-fractions from the same sample (Pevear, 1999; van der Pluijm et al., 2001). In previous work, it was shown that different size fractions contain different mixtures of detrital ($2M_1$) and authigenic ($1M_d$) illite. Note that authigenic illite in the shale layers is typically much finer and with different mineralogy than detrital grains, and is not readily observable in situ using optical and SEM analysis. The authigenic age of each sample was obtained using polytype quantification analyses for each size-fraction (supplementary Fig. A1). We plot the Ar-illite age vs. % $2M_1$ illite for each analyzed aliquot and calculate the age at 0 and 100% of $2M_1$ illite using the York regression analysis with improvements by Mahon (1996) to determine the age of detrital illite and authigenic illite. The statistics also allow estimation of the standard error of these ages (analytical-1σ and illite quantification). Lastly, the resulting ages at the tectonic front of the MFTB are compared with knowledge of the regional geology and stratigraphic constraints for the timing of deformation.

4. Results

The samples collected in the two limbs and hinge of Fold 1 (Fig. 2a) show no significant variations in mineralogical composition (illite/smectite, illite, kaolinite, calcite and quartz). The four different clay-size fractions of each sample show only minor variation in calcite concentration in the finer fractions and kaolinite in the coarser fractions (see Table 1). The illite properties (illite crystallinity-IC, crystallite size-CS and the % $2M_1$ illite) were determined for three clay size of samples 1-FL, 1-H and 1-BL, each of which was subsequently dated (see Fig. 2 and Table 1). The size fractions were 0.05–0.2, 0.2–1 and 1–2 microns in particle diameter, and are hereafter respectively referred to as fine-medium, medium-coarse, and coarse. The finest size fraction (<0.05 μm) could not be dated because it contained very small concentrations of illite, almost 100% of which was $1M_d$ illite. Consequently, our analysis uses three size-fractions greater than 0.05 microns. No other phase containing potassium was detected in the samples. XRD analyses show kaolinite as the dominant phase in the coarse fraction and illite in the coarse-medium and medium-fine, with increases in calcite content in the finer fractions (Table 1).

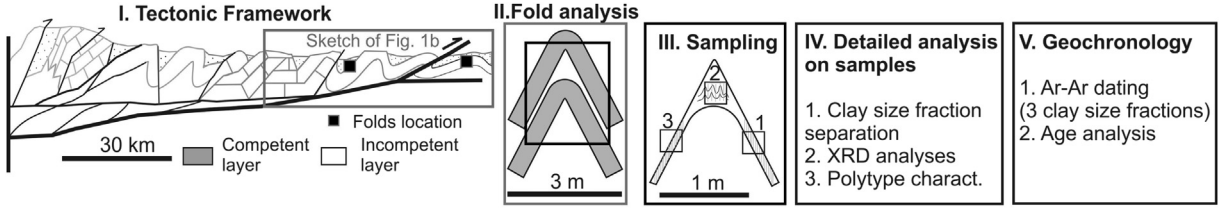

Fig. 3. The main steps of the fold-dating method. See text for explanation.

Table 1
Synthetic table showing the results of illite characterization with XRD analysis and ages determined in the analyzed samples.

Sample	Mineralogy	IC (2θ)	CS (nm)	% smectite in I/S	Age (Ma)		Clay size fraction	2M1 (%)
					RA	TGA		
1-FL	K, I/S, calcite and I	0.98	8.1	30	60.1 ± .9	48.7 ± 0.7	C	9 ± 2
	I/S, K and minor calcite	1.03	7.7	30	67.7 ± 0.9	46.8 ± 0.7	MC	7 ± 2
	Calcite, I/S and minor quartz	1.23	6.4	20	67.7 ± 0.9	45.5 ± 0.4	FM	4 ± 1
1-H	K, I/S, calcite and I	0.99	8.0	25	55.0 ± 0.5	47.9 ± 0.5	C	9 ± 2
	I/S, K and minor calcite	1.05	7.6	40	61.5 ± 0.3	47.3 ± 0.2	MC	7 ± 2
	Calcite, I/S and minor quartz	1.24	6.4	30	61.6 ± 0.5	43.9 ± 0.4	FM	1 ± 1
1-BL	K, I/S, calcite and I	1.01	7.9	30	58.9 ± 0.4	48.4 ± 0.3	C	10 ± 2
	I/S, K and minor calcite and quartz	1.06	7.5	40	84.2 ± 0.4	47.5 ± 0.2	MC	7 ± 2
	Calcite, I/S and minor quartz	1.31	6.1	25	79.1 ± 0.4	45.0 ± 0.2	FM	3 ± 1
2-FL	I, I/S, K and calcite	0.90	8.8	~20	81.6 ± 0.2	71.8 ± 0.2	C	18 ± 5
	I, I/S, K and calcite	1.09	7.4	~20	81.5 ± 0.3	67.4 ± 0.2	MC	7 ± 5
	Calcite and I/S	1.20	6.5	~20	89.3 ± 0.3	62.7 ± 0.2	FM	2 ± 5
2-H	I, chlorite, K and minor calcite	0.92	8.8	~15	89.8 ± 0.3	76.2 ± 0.3	C	24 ± 3
	I, chlorite and minor calcite	1.00	8.0	~10	92.8 ± 0.3	75.6 ± 0.3	MC	13 ± 3
	I, and minor calcite and chlorite	0.96	8.4	~15	91.5 ± 0.3	71.1 ± 0.2	FM	5 ± 3
2-BL	I, chlorite, K and minor calcite	0.94	8.5	~15	83.5 ± 0.3	73.1 ± 0.3	C	20 ± 3
	I, chlorite and minor calcite	1.19	6.8	?	87.7 ± 0.4	73.5 ± 0.3	MC	7 ± 3
	I, and minor calcite and chlorite	0.97	8.2	?	88.4 ± 0.3	68.6 ± 0.3	FM	4 ± 3

I/S = interestratified illite/smectite; K = kaolinite; I = discrete illite. IC = Illite Crystallinity Index-in degrees, calibrated (Warr and Rice, 1994), CS = Crystallite Size-in Angstrom calculated with Scherrer Equation (with $K = 0.9$ and $\lambda = 1.54$ Å). % Smectite determined with 001/002 and 002/003 reflections in glycoled samples (Table 8.3 in Moore and Reynolds, 1997). Clay size fractions: C = coarse, 1-2 μm-; MC = medium-coarse, 0.2 -1 μm-; FM = fine-medium, 0.05–0.2 μm. RA = Ar/Ar illite Retention Age; TGA = Ar/Ar illite Total Gas Age.

Analyses of XRD patterns measured in air-dried and glycolated samples show the presence of two illite polytypes and very small proportions of discrete illite and interstratified illite/smectite (I/S). An average of 35-20% smectite in these samples was determined with 001/002 and 002/003 reflections in the glycolated samples (Table 8.3 in Moore and Reynolds, 1997). Comparison of experimental XRD patterns from randomly oriented preparations with model WILDFIRE patterns (Solum et al., 2005; Haines and van der Pluijm, 2008) indicate that the discrete illite is $2M_1$, and the I/S contains $1M_d$ illite. Moreover, $2M_1$ illite is practically absent in the fine and medium fractions, representing approximately 7% in the medium-coarse and up to 9–10% in the coarse fractions in the three samples (Fig. A1). Illite is more crystalline (IC is smaller) and has thicker crystallites in the coarser size-fractions than in the finer fractions, and varies consistently in a range between 1 and 1.3 $\Delta 2\theta^\circ$ in the three analyzed samples. This composition represents crystallite sizes (CS) between 6 and 8 nm. Most of the Ar step-heating spectra show degassing paths and amounts of recoil (between 0.44 and 0.13 of the fraction of gas released) consistent with predictions from models of illite degassing by Dong et al. (1995, 1997, Table 1 and Fig. A2 in the supplements) and calculated crystallite sizes. The Ar total gas ages vary between 48.7 and 45.5 Ma, 47.9 and 43.9 Ma, and 48.4 and 45 Ma, for samples 1-FL, 1-H and 1-BL, respectively, with errors less than 0.7 Ma.

Similar to Fold 1, the mineralogies of the limbs and hinge of Fold 2 are alike. They contain, illite, calcite and minor chlorite, although chlorite is less abundant in the finer fractions of all clay-size fractions in sample 2-FL, where illite/smectite and greater amounts of calcite were also detected (Table 1). Following the method above, 5–20% smectite in I/S is present in these samples, being more abundant in samples from 2-FL. $2M_1$ illite polytype is present in less than 24% in the coarser fraction and is almost absent in the finer fractions (Fig. A1). The IC ranges between 0.9 and 1.2 $\Delta 2\theta^\circ$, with no systematic variation among the different size fractions, representing slightly larger crystallite size estimates (6.5 and 9 nm) than those from Fold 1. The Ar step-heating spectra show degassing paths and amounts of recoil (between 0.3 and 0.12 of the fraction of gas released) that are consistent with predictions from models of illite degassing by Dong et al. (1995, 1997, Table 1 and Fig. A2 in the supplements) and calculated crystallite sizes. The Ar total gas ages vary between 71.8 and 62.7 Ma, 71.1 and 76.2 Ma, and 68.6 and 73.5 Ma, for samples 2-FL, 2-H and 2-BL, respectively, with errors less than 0.4 Ma.

5. The age of folding

Polytype characterization in XRD patterns in Fold 1 samples show the dominance of $1M_d$ illite with only up to 10% of $2M_1$ illite in the coarser fraction, and close to zero in the finer fractions. Based upon the metamorphic conditions, we consider the $2M_1$ illite as detrital in origin and the low-temperature polytype $1M_d$ as authigenic illite (see also, Dong et al., 1995, 1997; Haines and van der Pluijm, 2008), that grew during deformation. Evidence for other potassium-bearing phases in these samples is absent, so the Ar ages of the analyzed samples correspond to illite polytypes mixed in different proportions for each of the clay-size fractions. The Ar vacuum-encapsulated illite dating method determines the Ar recoil and calculates both total gas ages and model-dependent retention ages that assume vacancy free illite (Dong et al., 1995). Based upon crystallite thickness estimates (<10 nm, Table 1), we use total gas ages for illite in these samples. All of the 9 ages from the 3 clay size-fractions in samples 1-FL, 1-H and 1-BL provide consistent Ar spectra, giving a range between 48.7 and 43.9 Ma from coarse to fine fractions, with analytical errors of ±0.7Ma. Ar spectra from all samples and size-fractions from Fold 2 are also similar (Fig. A2), providing an age range between 75.6 and 62.7 Ma with errors of 0.4 Ma.

The % $2M_1$ illite from XRD analyses are plotted against the Ar ages in Fig. 4. The ages and % of $2M_1$ from the analysed samples in Fold 1 fall almost perfectly on a line with a positive slope [$(\exp(\lambda^* t))^{-1} = 0.0003\%\ 2M_1 + 0.024$, $R^2 = 0.97$, Fig. 4]. York regression (Mahon, 1996) of these data results in an upper intersection (100% $2M_1$ illite) at 96.4 ± 9.2 Ma and a lower intersection (100% $1M_d$ illite) at 43.5 ± 0.3 Ma. The upper intersect records the age of detrital illite and the lower intersect corresponds to the age of authigenic illite. However, because samples have less than 10% of $2M_1$ illite (i. e., they are dominated by authigenic illite), the reliability of the upper intersect and, therefore, the extrapolated age of the detrital illite, is not well-constrained.

Data from Fold 2 also fall along a mixing line in the % $2M_1$ vs. Ar ages space, but the line is steeper and the ages show slightly more

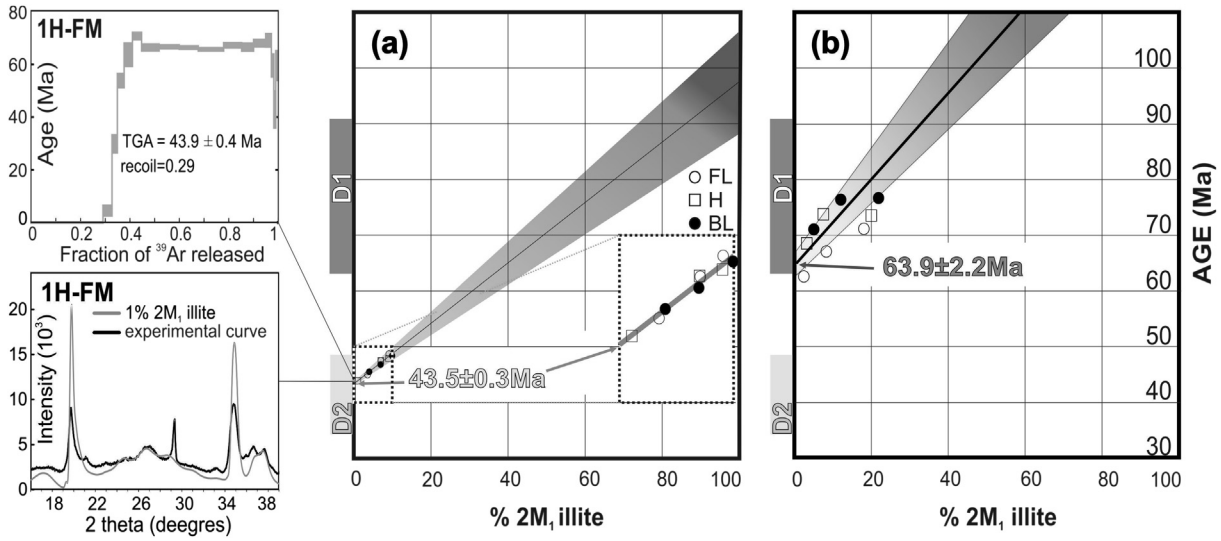

Fig. 4. (a) Plot of % $2M_1$ vs. Ar illite total-gas ages of the different clay-size fractions in samples 1-FL, 1-H and 1-BL of Fold 1. The error estimates of the intersections at 0 and 100% $2M_1$ were determined using Mahon (1996). Notice the almost perfect correlation of results along the mixing line, magnified on the lower right. On the left is a representative Ar degassing spectrum and the associated XRD plot (2θ vs. intensity) with WILDFIRE modeling that best fits the pattern of the fine-medium fraction of this sample (1-H FM). On the y axis, the permissible stratigraphic age ranges for D1 and D2 are indicated, constraining the calculated intercept from Ar dating. (b) Plot of % $2M_1$ vs. Ar illite total gas ages from Fold 2. As in Fold 1, results are also distributed along a mixing line with slightly greater dispersion. Ages of deformation, at 0% $2M_1$, is indicated.

dispersion [$(\exp(\lambda^* t))^{-1} = 0.002\%\ 2M_1 + 0.037$, $R^2 = 0.55$, Fig. 4]. York regression of these data results in an upper intersection (100% $2M_1$ illite) at 132.8 ± 15.2 Ma and a lower intersection at 63.9 ± 2.2 Ma.

Previous work in the area has shown that the MFTB experienced two major deformation phases; the first, D1, ending around the Cretaceous-Tertiary boundary in the TMB, as suggested by an angular unconformity between Maastrichtian flysch and Paleocene molasse deposits, and a second phase, D2, that folded the K-T unconformity in the frontal segment (Fitz-Díaz et al., 2012). The D2 deformation event has also been extensively documented along the Gulf of Mexico based upon surface observations, borehole records and analyses of seismic lines. It has been constrained between Middle Eocene to Oligocene (approx. 48–30 Ma) based upon stratigraphic analysis of clastic units in the Gulf of Mexico coastal plain (Roure et al., 2009; Alzaga-Ruíz et al., 2009 and references therein). The age of the lower intersect of the mixing line (43.5 ± 0.3 Ma, Fig. 4) of Fold 1 falls well within the permissible stratigraphic range for D2, showing that illite precipitation reflects the timing of processes associated with folding in this part of the area. The age of the lower intercept of Fold 2 in the same tectonic basin setting to the west is considerably older (63.9 ± 2.2 Ma) and coincides with the proposed age range of D1 in the area that involves the Mendez Fm., which has been well constrained (López-Oliva et al., 1999). The position of the studied folds in the MFTB, Fold 1 to the east and Fold 2 to the hinterland, and the difference in age obtained in them, Fold 2 being 20 million years older than Fold 1, imply a progressive but discontinuous propagation of deformation toward the foreland of the MFTB in the Paleogene.

6. Conclusions

We propose a method that can determine the absolute age of folds that were formed at very low metamorphic grades by combining clay characterization and quantification with Ar-encapsulation dating of submicroscopic illite grain size fractions. Applying this approach to folds in the Tampico-Misantla Basin of Mexico results in well-defined ages of 44 Ma and 64 Ma that match more broadly-defined local and regional stratigraphic constraints for the timing of deformation in this part of the Mexican Fold-Thrust Belt. The distinctly different ages of folds developed in the same stratigraphic horizon from the same basin demonstrate that these illite ages are not regional diagenetic events, but that they are restricted to local areas of deformation, in this case represented by folding.

In addition to constraining of the timing of folding in deformation belts, this method also has potential to determine rates of deformation, and to track the propagation of deformation across and along foreland orogenic belts in Mexico and elsewhere.

Acknowledgments

This work benefited from field collaboration with Gustavo Tolson, who first introduced us to the wonderful outcrops in this part of the Mexican Fold Thrust Belt and insights from Peter Hudleston on fold kinematics. Ar ages and clay characterization were obtained at the University of Michigan; we thank Chris Hall and Anja Schleicher for technical support and stimulating discussions. Research was supported by a U-M Turner Postdoctoral Fellowship to EFD and National Science Foundation grants EAR 1118704 and 1216750 (BvdP). We thank Mark Fisher, and anonymous reviewer and editor William Dunne for reviews and comments that significantly improved the paper.

Appendix A. Supplementary data

Supplementary data related to this article can be found at http://dx.doi.org/10.1016/j.jsg.2013.05.011.

References

Alzaga-Ruiz, H., Lopez, M., Roure, F., Séranne, M., 2009. Interactions between the Laramide Foreland and the passive margin of the Gulf of Mexico: Tectonics and sedimentation in the Golden Lane area, Veracruz State, Mexico. Marine and Petroleum Geology 26, 951–973.

Cardwell, R.K., Chinn, D.S., Moore, G.F., Turcotte, D.L., 1978. Frictional heating on a fault zone with finite thickness. Geophysical Journal of the Royal Astronomical Society 52, 525–530.

Clauer, N., Srodon, J., Francu, J., Sucha, V., 1997. K-Ar dating of illite fundamental particles separated from illite-smectite. Clay Minerals 32, 181–196.

Clauer, N., Liewig, N., Ledesert, B., Zwingmann, H., 2008. Thermal history of Triassic sandstones from the Vosges Mountains-Rhine Graben rifting area, NE France, based on K-Ar illite dating. Clay Minerals 43, 363–379.
Dahlen, F.A., Barr, T.D., 1989. Brittle frictional mountain building 1: deformation and mechanical energy Budget. Journal of Geophysical Research 94, 3923–3947.
Dong, H., Hall, C.M., Halliday, A.N., Peacor, D.R., Merriman, R.J., Roberts, B., 1997. $^{40}Ar/^{39}Ar$ of Late Caledonian (Acadian) metamorphism and cooling of K-bentonites and slates from the Welsh Basin, U.K. Earth and Planetary Science Letters 150, 337–351.
Dong, H., Hall, C.M., Peacor, D.R., Halliday, A.N., 1995. Mechanisms of argon retention in clays revealed by laser ^{40}Ar-^{39}Ar dating. Science 267, 355–359.
Fitz-Díaz, E., Hudleston, P., Tolson, G., 2011a. Comparison of tectonic styles in the Mexican y Canadian Rocky mountain fold-thrust belt. In: Poblet, J., Lisle, R. (Eds.), Special Publication on Kinematics y Tectonic Styles of Fold-thrust Belts 349. Geological Society of London, pp. 149–167.
Fitz-Díaz, E., Hudleston, P., Kirschner, D., Siebenaller, L., Camprubi, T., Tolson, G., Pi-Puig, T., 2011b. Insights into fluid flow and water-rock interaction during deformation of carbonate sequences in the Mexican fold-thrust belt. Journal of Structural Geology 33, 1237–1253.
Fitz-Diaz, E., Tolson, G., Hudleston, P., Bolanos-Rodriguez, D., Ortega-Flores, B., Serrano, A.V., 2012. The role of folding in the development of the Mexican fold-and-thrust belt. Geosphere 8, 931–949.
Gray, G.G., Pottorf, R.J., Yurewicz, D.A., Mahon, K.I., Pevear, D.R., Chuchla, R.J., 2001. Thermal and chronological record of syn-to post-Laramide burial and exhumation, Sierra Madre Oriental, Mexico. AAPG Memoir 75, 159–181.
Haines, S., van der Pluijm, B., 2008. Clay quantification and Ar dating of synthetic and natural gouge: application to the Miocene Sierra Mazatlán detachment fault, Sonora, Mexico. Journal of Structural Geology 30, 525–538.
Hobbs, B.E., Ord, A., Regenauer-Lieb, K., 2011. The thermodynamics of deformed metamorphic rocks: a review. Journal of Structural Geology 33, 758–818.
Hudleston, P., Treagus, S., 2010. Information from folds: a review. Journal of Structural Geology 32, 2042–2071.
Kübler, B., 1968. Évaluation quantitative du métamorphisme para la cristallinité de l'illite; état des progrès realisés ces dernières années. Centre de Recherches de Pau (Societé Nationale des Petôoles d'Aquitaine 2, 385–397.
López-Oliva, J.G., Keller, G., Stinnesbeck, W., 1999. El limite Cretacico/Terciario (K/T) en el noreste de Mexico, extincion de foraminiferos planctonicos. The Cretaceous-Tertiary boundary in northeastern Mexico, extinction of planktonic Foraminifera. Revista Mexicana de Ciencias Geologicas 15, 109–113.
Mahon, K., 1996. The new "York" regression; application of an improved statistical method to geochemistry. International Geology Review 38, 293–303.
Merriman, R.J., Peacor, D.R., 1999. Very-low grade metapelites: mineralogy, microfabrics and measuring reaction progress. In: Frey, M., Robinson, D. (Eds.), Low-grade Metamorphism. Blackwell Science, UK, pp. 10–60.
Moore, D.M., Reynolds Jr., R.C., 1997. X-ray Diffraction and the Identification and Analysis of Clay Minerals. Oxford University Press, Oxford, United Kingdom, p. 373.
Ortega-Flores, B., 2011. Deformación por acortamiento en la Plataforma Valles-San Luís Potosí y en la Cuenca Tampico-Misantla; porción externa del Cinturón de Pliegues y Cabalgaduras Mexicano. Masters thesis. Universidad Nacional Autónoma de México.
Pessagno Jr., E.A., 1969. Upper Cretaceous stratigraphy of the western Gulf Coast area of Mexico, Texas and Arkansas. Geological Society of America Memoir 111, 1–139.
Pevear, D.R., 1999. Illite and hydrocarbon exploration. Proceedings of the National Academy of Sciences 96, 3440–3446.
Ramsay, J.G., 1974. Development of chevron folds. Geological Society of America Bulletin 85, 1741–1754.
Reynolds Jr., R.C., 1992. X-ray diffraction studies of illite/smectite from rocks, $<1\mu m$ randomly oriented powders, and $<1\mu m$ oriented powder aggregates; the absence of laboratory-induced artifacts. Clays and Clay Minerals 40, 387–396.
Roure, F., Alzaga-Ruiz, H., Callot, J., Ferket, H., Granjeon, D., Gonzalez-Mercado, G.E., Guilhaumou, N., Lopez, M., Mougin, P., Ortuno-Arzate, S., Seranne, M., 2009. Long lasting interactions between tectonic loading, unroofing, post-rift thermal subsidence and sedimentary transfers along the western margin of the Gulf of Mexico: Some insights from integrated quantitative studies. Tectonophysics 475, 169–189.
Rousset, D., Clauer, N., 2003. Discrete clay diagenesis in a very low-permeable sequence constrained by an isotopic (K–Ar and Rb–Sr) study. Contributions to Mineralogy and Petrology 145, 182–198.
Solum, J.G., van der Pluijm, B.A., Peacor, D.R., 2005. Neocrystallization, fabrics and age of clay minerals from an exposure of the Moab Fault, Utah. Journal of Structural Geology 27, 1563–1576.
Surace, I.R., Clauer, N., Thélin, P., Pfeifer, H.R., 2011. Structural analysis, clay mineralogy and K–Ar dating of fault gouges from Centovalli Line (Central Alps) for reconstruction of their recent activity. Tectonophysics 510, 80–93.
Suter, M., 1987. Structural traverse across the Sierra Madre Oriental fold-thrust belt in east-central Mexico. Geological Society of America Bulletin 98, 249–264.
van der Pluijm, B.A., Hall, C.M., Vrolijk, P.J., Pevear, D.R., Covey, M.C., 2001. The dating of shallow faults in the earth's crust. Nature 412, 172–175.
Verdel, C., van der Pluijm, B., Niemi, N., 2011. Variations in the illite to muscovite transition related to metamorphic conditions and detrital muscovite content; insight from the Paleozoic passive margin of the southwestern United States. Journal of Geology 119, 419–437.
Vrolijk, P., van der Pluijm, B.A., 1999. Clay gouge. Journal of Structural Geology 21, 1039–1048.
Warr, L.N., Rice, A.H.N., 1994. Interlaboratory standardization and calibration of clay mineral crystallinity and crystallite-size data. Journal of Metamorphic Geology 12, 141–152.